J Mater Sci (2008) 43:2077–2081
DOI 10.1007/s10853-007-2432-x

LETTER

Mode-II shielding-curve of Al_2O_3 from measurement of cone crack angles

Theo Fett · Gabriele Rizzi · Michael J. Hoffmann · Rainer Oberacker · Susanne Wagner

Received: 31 October 2007 / Accepted: 26 December 2007 / Published online: 20 January 2008

Many ceramic materials exhibit the effect of an increasing crack growth resistance during crack extension. Especially in the case of coarse-grained materials, cracks generally follow the grain boundaries, leave the original crack plane and produce a crack-face roughness. In the theoretical analysis forces transmitted by local links between the two crack faces are smoothed and replaced by so-called continuous bridging stresses acting against the crack opening. As the consequence of such bridging stresses, there exists a shielding stress intensity factor term that shields the crack tip partially from the applied loads. This effect as a reason for the occurrence of R-curves is well documented in literature for cracks under pure mode-I loading conditions [1].

In addition it has to be expected that crack-face interactions will also affect crack extension under pure or superimposed mode-II loading as for instance outlined in literature for frictional crack-face interactions [2–4]. In [5] it was outlined that the shear tractions generated under small mode-II load contributions may cause a disappearing effective crack-tip stress intensity factor $K_{\mathrm{II,tip}}$. Also the externally applied mode-II stress intensity factor $K_{\mathrm{II,appl}}$ can be reduced by the mode-II shielding so that a disappearing $K_{\mathrm{II,tip}}$ can occur.

The distribution of the intensity of crack-face interlocking has the same consequences on the bridging tractions normal to the crack face σ_{br} as for the tangentially transferred tractions τ_{br}. At the same distance from the crack tip where the bridging interactions disappear, both the shear and the normal stresses must vanish. Under the assumption of the same traction versus displacement characteristics, the two stresses are proportional

$$\tau(x) = \lambda\, \sigma_{\mathrm{br}}(x) \tag{1}$$

with the crack coordinate x as shown in Fig. 1a.

The mode-II shielding stress intensity factor can be computed from the distribution of the shear tractions over the crack. It holds by use of the mode-II weight function h_{II}

$$K_{\mathrm{II,sh}} = \int_{a_0}^{a} \tau(x)\, h_{\mathrm{II}}(x)\, dx \tag{2}$$

For small scale considerations with the crack-face interactions concentrated near the crack tip, exclusively the asymptotic singular part of the weight function is of interest. This part is identical for mode-I and mode-II (see e.g., [6])

$$h_{\mathrm{II}} = h_{\mathrm{I}} = \sqrt{\frac{2}{\pi(a-x)}} \tag{3}$$

From (1) to (3) it simply results

$$K_{\mathrm{II,sh}} = \lambda\, K_{\mathrm{I,sh}} \tag{4}$$

Let us now apply this general relation to two possible bridging relations. A simple bridging relation that fulfills the required properties reads [7]

$$\sigma_{\mathrm{br}} = \sigma_0 \exp(-\delta_y/\delta_{y0}) \tag{5}$$

with a characteristic stress value $\sigma_0 < 0$ and a characteristic normal displacement δ_{y0}. It is plotted in Fig. 2a as the solid

T. Fett · G. Rizzi
Institut für Materialforschung II, Forschungszentrum Karlsruhe, Karlsruhe, Germany

T. Fett (✉) · M. J. Hoffmann · R. Oberacker · S. Wagner
Institut für Keramik im Maschinenbau, Universität Karlsruhe, Karlsruhe, Germany
e-mail: theo.fett@ikm.uni-karlsruhe.de

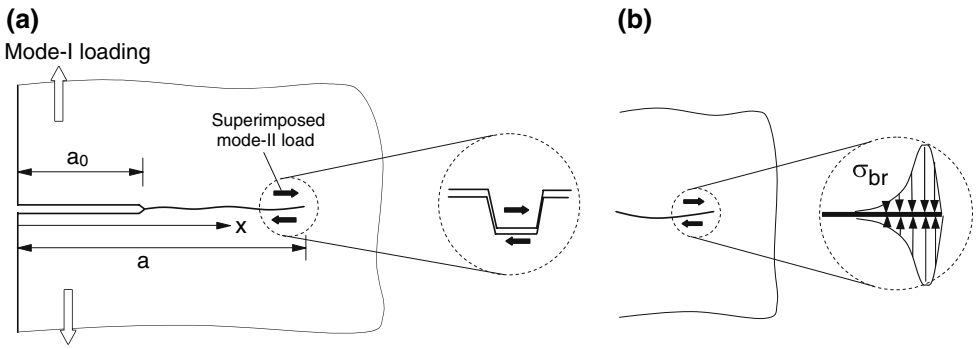

Fig. 1 Crack grown from a notch, (**a**) geometrical data, loading, and shielding against shear deformation by bridging interactions, (**b**) Modeling of crack-face interactions by interlocking under loading with bridging stresses

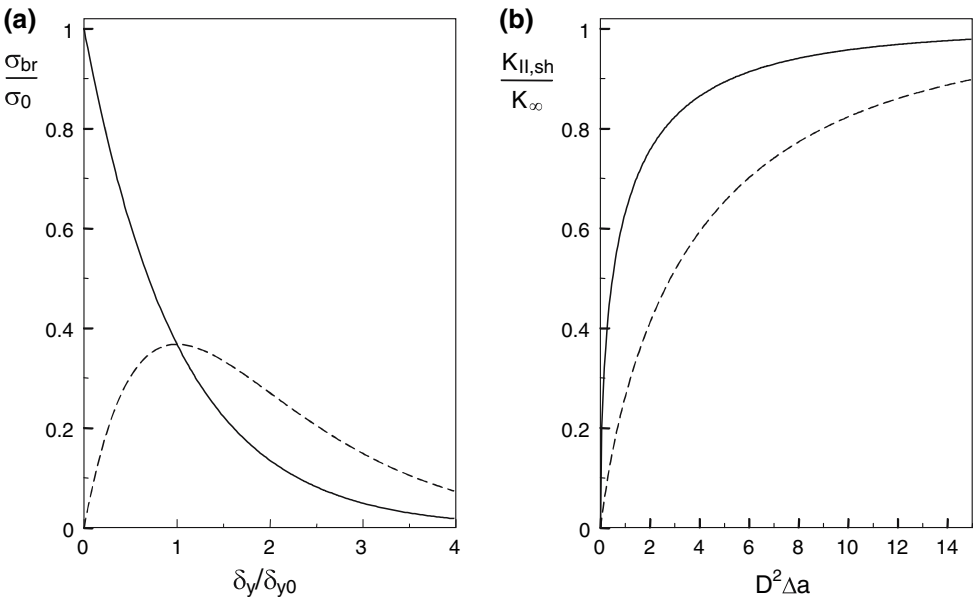

Fig. 2 (**a**) Two bridging stress dependencies, (**b**) related mode-II stress intensity factors; solid curves: Eqs. 5 and 8, dashed curves: Eqs. 10 and 11

curve. Under near-tip conditions the displacements δ_y during stable crack extension, can be expressed by the Irwin relation (for geometrical data see Fig. 1a)

$$\delta_y = \sqrt{\frac{8}{\pi}}\frac{K_{I0}}{E'}\sqrt{a-x} \tag{6}$$

where K_{I0} is the so-called crack-tip toughness and E' is the plane strain modulus. The shear tractions therefore read

$$\tau(x) = \sigma_0\,\lambda\exp[-D\sqrt{a-x}], \quad D = \sqrt{\frac{8}{\pi}}\frac{K_{I0}}{\delta_{y0}E'} \tag{7}$$

The evaluation of (2) results in

$$K_{II,sh} = \frac{\sigma_0\lambda}{D}\sqrt{\frac{8}{\pi}}[1-\exp(-D\sqrt{a-a_0})] \tag{8}$$

with the maximum shielding stress intensity factor

$$K_\infty = \frac{\sigma_0\lambda}{D}\sqrt{\frac{8}{\pi}} \tag{9}$$

The relation (8) is given in Fig. 2b by the solid curve. The sign of K_∞ has to be chosen so that $K_{II,sh}$ acts *against* the applied mode-II stress intensity factor.

A further bridging relation is [7]

$$\sigma_{br} = \sigma_0\frac{\delta_y}{\delta_{y0}}\exp(-\delta_y/\delta_{y0}) \tag{10}$$

plotted in Fig. 2a as the dashed curve. This set-up results in

$$K_{II,sh} = K_\infty[1-(1+D\sqrt{a-a_0})\exp(-D\sqrt{a-a_0})] \tag{11}$$

This dependency is illustrated in Fig. 2b as the dashed curve. The actual mode-II crack-tip stress intensity factor $K_{II,tip}$ results from

$$K_{II,tip} = \begin{cases} 0 & \text{for} \quad K_{II,appl}+K_{II,sh} \le 0 \\ K_{II,appl}+K_{II,sh} & \text{else} \end{cases} \tag{12}$$

This stress intensity factor governs the local stability of crack paths. If the value $K_{II,tip}$ does not disappear, the crack must kink by an angle of Θ out of the initial crack plane

and will propagate then under $K_{II,tip} = 0$. For small values of $K_{II,tip}/K_{I0}$, the crack kink angle Θ can be expressed by [8]

$$\Theta = -2\frac{K_{II,tip}}{K_{I0}} \tag{13}$$

Whereas the material parameter D can be computed from available material data by Eq. 7, the parameter K_∞ has to be determined experimentally by an appropriate experiment.

In [9] first measurements on K_{IIR} were reported but not evaluated with respect to the parameters of a special model. A commercial alumina, Frialit F99.7 (Friatec, Friedrichsfeld), with a median grain size of $d_m \approx 9$ μm was tested. Specimens of $3 \times 4 \times 45$ mm^3 were loaded by the force P via two opposite spheres of radius $R = 5$ mm (Fig. 3a). Tests under monotonously increasing load were performed up to varying maximum loads. The specimens were cut through the center of the contact area. Under the SEM, the main crack dimensions were measured (Fig. 3b). For the slightly scattering cone angles an average value of $\alpha = 31°$ was found (for more experimental details see [5]).

Stress intensity factor computations require 3D analysis. For the determination of the applied stress intensity factors, 3D finite element computations were performed. A finite element mesh of about 700 elements with 2,500 nodes was applied. The crack-tip region was modeled by collapsed two-dimensional elements. Computations for a cone crack angle of $\alpha = 31°$ as an average value for 15 specimens were carried out using ABAQUS, Version 6.2. The resulting stress intensity factors are plotted in Fig. 4 for several cone angles and crack lengths a.

A significant mode-II stress intensity factor contribution was obtained. Slightly depending on the crack lengths, the applied stress intensity factor $K_{II,appl}$ disappears at $\alpha = 27$–$28°$. The measured angle was different, namely $\alpha = 31°$. In this context it has to be emphasized that the

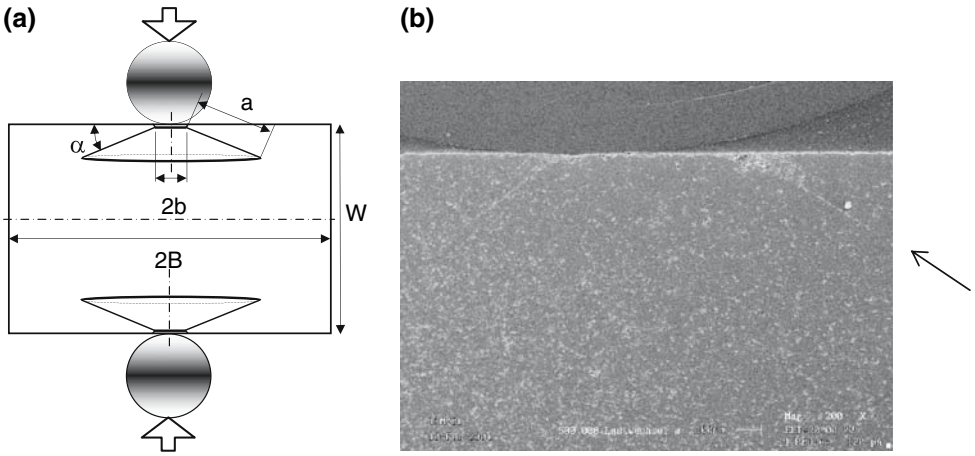

Fig. 3 (**a**) Opposite cone cracks in a rectangular bar (geometric data), (**b**) cross-section through a cone crack

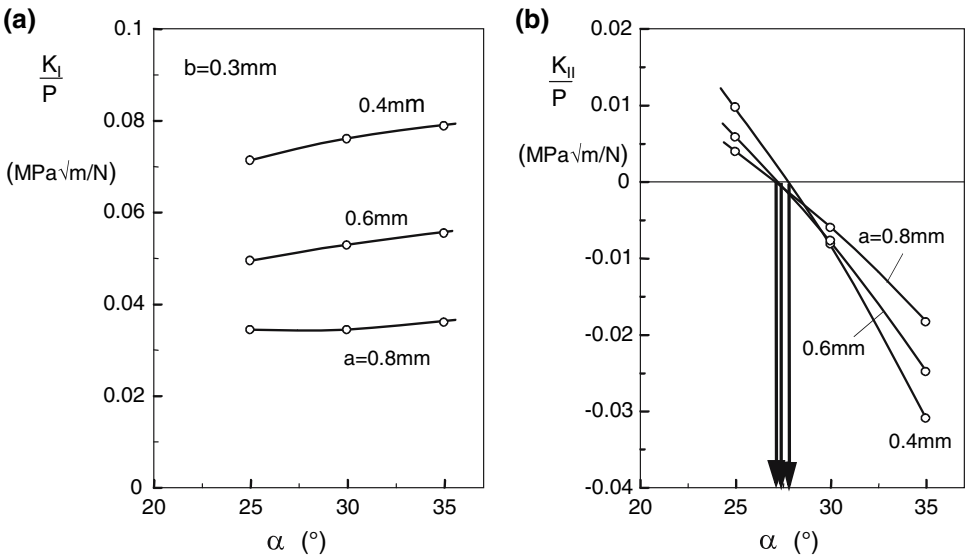

Fig. 4 Influence of geometric data on the mixed-mode stress intensity factors for opposite cone cracks, (**a**) Mode-I, (**b**) Mode-II stress intensity factors, arrow: cone angles for $K_{II,appl} = 0$

finite element result for the loading by two opposite spheres must differ from those obtained for a single sphere acting on an elastic half-space for which for example $K_{II,appl}$ disappears at $\alpha = 18–21°$ depending on Poisson's ratio ν.

From the maximum force P in the tests under continuously increasing load and the dimensions of the generated cone cracks, the shielding stress intensity factors at the different crack lengths can be determined. Figure 5a shows the mode-I shielding stress intensity factor data determined from the microscopically measured crack lengths a and applied load P by finite element computations. It has to be considered that the scatter in data is caused by the application of a multi-specimen test and not the result of one single propagating crack at different crack lengths. The initial value of the R-curve, $K_{I0} = 2.2$ MPa$\sqrt{}$m, was taken from [10]. With this value an increase of the R-curve up to $K_{IR} \cong 7–8$ MPam$^{1/2}$ can be stated.

As can be seen from Fig. 5b, a mode-II stress intensity factor resulting from the applied loading exists. On the other hand, it is obvious that the crack is straight and, consequently, $K_{II,tip} = 0$. This condition was fulfilled in all observations as for example can be seen from the image of Fig. 3b.

The mode-II shielding contribution can now be determined from the disappearing mode-II crack-tip stress

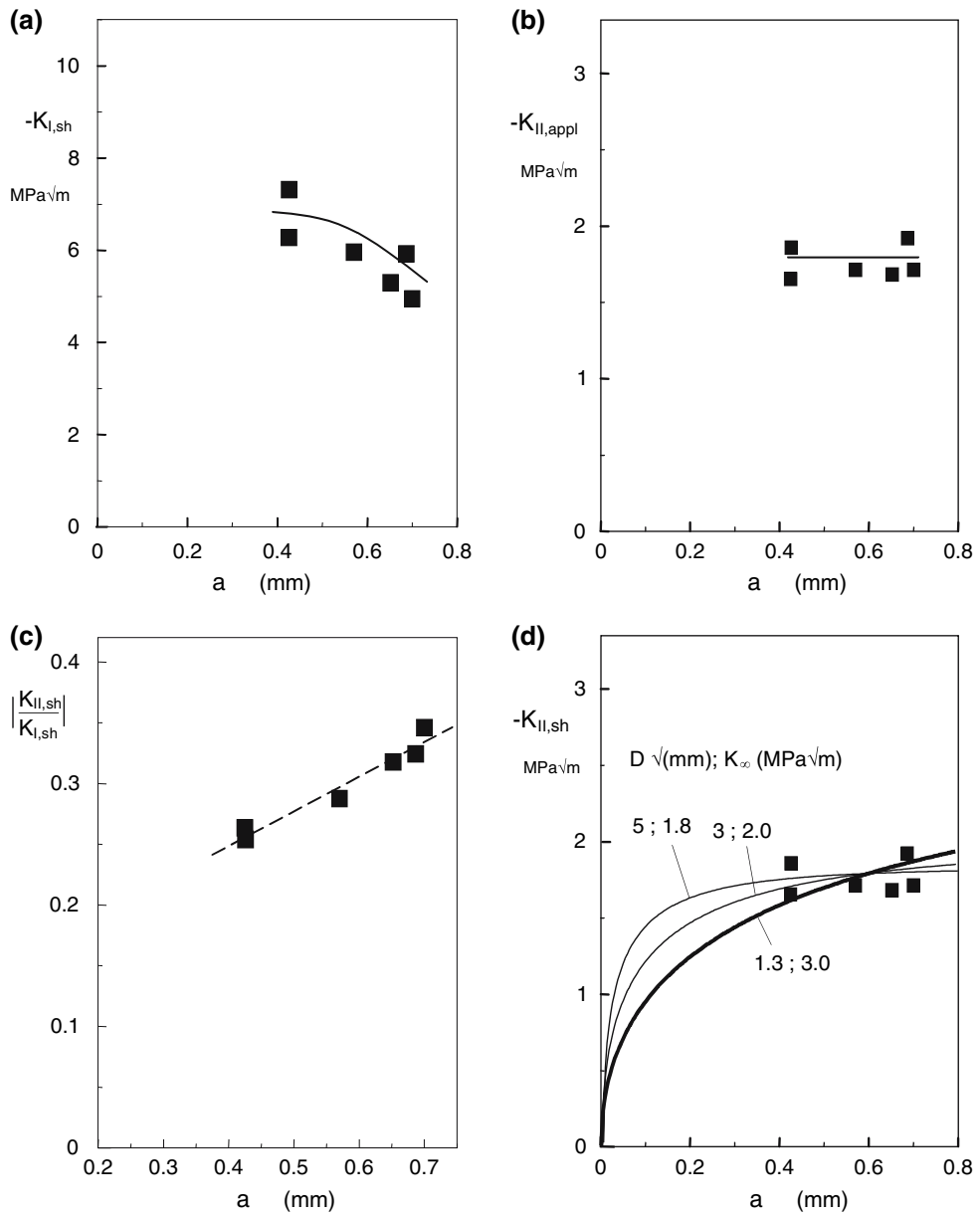

Fig. 5 (**a**) Shielding stress intensity factor $K_{I,sh}$(c), (**b**) applied mode-II stress intensity factor, (**c**) ratio of shielding terms versus crack length, (**d**) mode-II shielding curves obtained by fitting Eq. 8 to the experimental data

intensity factor and the observed finite $K_{II,appl}$. The cone angle result of $\alpha = 31°$ found in our experiments differs from that expected from the condition of $K_{II} = 0$. From this it can be concluded that a shielding mode-II stress intensity factor contribution leads to an increase in the cone angle. The individual values of the ratio $K_{II,sh}/K_{I,sh}$ are given in Fig. 5c. The ratio of the two shielding terms is roughly 0.3, but shows an increase with increasing crack length. In this context it should be noted that a constant ratio predicted by Eq. 4 was derived under the assumption of an identical weight function for mode-I and mode-II crack-face loading. The two weight functions are trivially the same for near-tip loading, as shown in [6].

The total disappearing stress intensity factor is given by Eq. 12. This relation allows the mode-II shielding stress intensity factor to be determined as shown by the symbols in Fig. 5d. By fitting Eq. 8 to the data points of Fig. 5d the parameter K_∞ is obtained for a given value of the second parameter D. As a result, the pairs of parameters noted at the curves in Fig. 5d were obtained. In this context, it should be noted that the K_{II}-R-curve for finite cracks can only be roughly represented by use of the near-tip solution (8). The reason is the occurrence of higher-order terms in the weight function which depend on geometry of crack and component.

In literature, data for the characteristic bridging parameter δ_{y0} obtained with macroscopic cracks are available for coarse-grained alumina. The data obtained from macroscopic cracks are about $\delta_{y0} \leq 0.25$ μm. For $K_{I0} = 2.2$ MPa$\sqrt{\text{m}}$, $E' = 350$ GPa, and the value of $\delta_{y0} = 0.25$ μm [11] it results from Eq. 6 $D \cong 1.3/\sqrt{(\text{mm})}$. Also this value was used in the fit procedure. The maximum shielding stress intensity factor K_∞ is found to be in the range of 1.8–3 MPa$\sqrt{\text{m}}$. In addition two curves for modified sets of parameters are entered in Fig. 5d.

The maximum mode-II shielding stress intensity factor K_∞ is roughly 1/4–1/2 of the mode-I shielding stress intensity factor of $K_\infty = K_{IR}$–$K_{I0} \approx$ 5–6 MPa$\sqrt{\text{m}}$. This means that the coefficient in (1) becomes $|\lambda| \approx$ 1/4–1/2.

References

1. Munz D (2007) J Am Ceram Soc 90:1
2. Mendelsohn DA, Gross TS, Zhang Y (1995) Acta metall mater 43(3):893
3. Mendelsohn DA, Gross TS, Goulet RU, Zhouc M (1998) Mater Sci Eng A249:1
4. Lathabai S, Rödel J, Lawn BR (1991) J Am Ceram Soc 74:1340
5. Fett T, Rizzi G, Munz D, Hoffmann M, Oberacker R, Wagner S (2006) J Ceram Soc Jpn 114:1038
6. Rice JR (1972) Int J Solids Struct 8:751
7. Munz D, Fett T (1999) CERAMICS, failure, material selection, design. Springer-Verlag, Heidelberg
8. Cotterell B, Rice JR (1980) Int J Fract 16:155
9. Fett T, Rizzi G, Munz D, Badenheim D, Oberacker R (2006) Fatigue Fract Eng Mater Struct 29:867
10. Kounga Njiwa AB, Yousef GS, Fett T, Rödel J (2005) Eng Fract Mech 72:1011
11. Fett T, Munz D, Thun G, Bahr HA (1995) J Amer Ceram Soc 78:949